Received: 3 August 2017 | Revised: 6 September 2017 | Accepted: 9 September 2017

DOI: 10.1002/aoc.4126

FULL PAPER

WILEY Applied Organometallic Chemistry

Three new mixed-ligand copper(II) complexes containing glycyl-L-valine and N,N-aromatic heterocyclic compounds: Synthesis, characterization, DNA interaction, cytotoxicity and antimicrobial activity

Yong-Yu Qi[1] | Ya-Xian Liu[1] | Qian Gan[1] | Ya-Hong Xiong[1] | Zong-Wan Mao[1,2] | Xue-Yi Le[1]

[1]Department of Applied Chemistry, South China Agricultural University, Guangzhou 510642, People's Republic of China

[2]School of Chemistry and Chemical Engineering, Sun yat-sen University, Guangzhou 510275, People's Republic of China

Correspondence
Xue-Yi Le, Department of Applied Chemistry, South China Agricultural University, Guangzhou 510642, People's Republic of China.
Email: lexyfu@163.com

Funding information
Natural Science Fund, Grant/Award Number: 2015A030313423; College Students' Innovation and Entrepreneurship Training Program in Guangdong, Grant/Award Number: 1056413042

Three novel copper(II) complexes, $[Cu(Gly\text{-}L\text{-}Val)(HPBM)(H_2O)]\cdot ClO_4\cdot H_2O$ (**1**), $[Cu(Gly\text{-}L\text{-}Val)(TBZ)(H_2O)]\cdot ClO_4$ (**2**) and $[Cu(Gly\text{-}L\text{-}Val)(PBO)(H_2O)]\cdot ClO_4$ (**3**) (Gly-L-Val = glycyl-L-valine anion, HPBM = 5-methyl-2-(2′-pyridyl)benzimidazole, TBZ = 2-(4′-thiazolyl)benzimidazole, PBO = 2-(2′-pyridyl)benzoxazole), have been prepared and characterized with elemental analyses, conductivity measurements as well as various spectroscopic techniques. The interactions of these copper complexes with calf thymus DNA were explored using UV–visible, fluorescence, circular dichroism, thermal denaturation, viscosity and docking analyses methods. The experimental results showed that all three complexes could bind to DNA via an intercalative mode. Moreover, the cytotoxic effects were evaluated using the MTT method, and the antimicrobial activity of these complexes was tested against *Bacillus subtilis*, *Staphylococcus aureus*, *Escherichia coli* and *Pseudomonas aeruginosa*. The results showed that the activities are consistent with their DNA binding abilities, following the order of **1** > **2** > **3**.

KEYWORDS
antimicrobial activity, copper(II) complexes, cytotoxicity, DNA interaction, Gly-L-Val

1 | INTRODUCTION

During recent years metal complexes as DNA molecule probes and chemotherapeutic reagents have attracted considerable attention.[1–4] Under most circumstances, metal ions act as an inorganic modifier of the organic backbone of bioactive molecules and ligands endowing DNA affinity and specificity.[5] Among transition metals, copper has good coordination properties and its complexes have shown encouraging potential, given that many of them display favorable photo-cleavage activity and various bioactivities such as antibacterial, antitumor and anti-inflammatory activities.[3,6,7]

In these copper(II) complexes, chemical and biological activities are greatly affected by a ligand. A change of the substituent properties and binding site of the ligand can cause certain differences in the spatial configuration and electron cloud density distribution of the complexes, resulting in differences in DNA binding properties or bioactivities.[8–12] Very recently, Kumar and co-workers have observed that copper(II) complexes exhibit effective anticancer and antimicrobial activity via strongly binding and cleaving DNA, and the activity of the complexes varied with the ligand.[13–15] Thus, studies of the differences can be favorable for thoroughly understanding the binding mechanism of copper complexes to DNA. So far, particular

attention has been primarily focused on copper(II) complexes containing N,N-aromatic heterocyclic compounds due to their high DNA binding ability[16] and antiphlogistic,[17] antibacterial[18] and antitumor activities.[19,20] Moreover, numerous copper complexes with various modified N,N-aromatic heterocyclic compounds have been synthesized, and their DNA binding and cleavage activities have also been explored.[21,22]

Dipeptides, acting as structural units of proteins and related metabolites, have been commonly used as hormones, immunomodulators, enzyme inhibitors and neurotransmitters in living systems.[23,24] Based on the above-mentioned properties, copper complexes with dipeptides have been investigated as models for both protein–DNA and antitumor agent–DNA interactions.[25–27] Consequently, it is meaningful to gain some insight into the DNA interaction, antibacterial and antitumor properties of copper complexes with N,N-aromatic heterocyclic compounds and dipeptides.

In our previous works, we have reported a series of copper(II) peptide complexes containing N,N-aromatic heterocyclic compounds,[28–34] and also studied their DNA interactions, antioxidation properties and cytotoxicity. It was found that the ligands have significant influence on the activities. Among them, copper(II) complexes containing glycyl-L-valine (Gly-L-Val) and 2-(2′-pyridyl)benzimidazole exhibited high nucleobase affinity and nuclease activity and had potential to serve as anticancer agents.[34] However, the antibacterial activity of these complexes has been neglected and little systematic investigation has been made into the effect of the structure of N,N-aromatic heterocyclic ligands on the activities.

As an extension of these previous works, we have synthesized three new complexes of similar type: [Cu(Gly-L-Val)(HPBM)(H_2O)]·ClO_4·H_2O (**1**), [Cu(Gly-L-Val)(TBZ)(H_2O)]·ClO_4 (**2**) and [Cu(Gly-L-Val)(PBO)(H_2O)]·ClO_4 (**3**) (HPBM = 5-methyl-2-(2′-pyridyl)benzimidazole, TBZ = 2-(4′-thiazolyl)benzimidazole, PBO = 2-(2′-pyridyl)benzoxazole). UV–visible and fluorescence spectroscopies were applied to determine the strength of interaction between the complexes and calf thymus DNA (CT-DNA). Further experiments, including viscosity, circular dichroism (CD), thermal denaturation and docking analyses, were carried out to assess the binding modes. In order to evaluate the biological properties of the complexes, we investigated their DNA cleavage abilities via gel electrophoresis measurements. Furthermore, the cytotoxicities against A549 (human lung carcinoma), HeLa (human cervical carcinoma) and PC-3 (human prostate carcinoma) cell lines and 3 T3 (mouse embryonic fibroblast) cells were determined using 3-(4,5-dimethylthiazol-2-yl)-2,5-diphenyltetrazolium bromide (MTT) assay and the antibacterial activities of the complexes were measured using the agar diffusion method and double broth dilution method. The results showed that the structures of the N,N-aromatic heterocyclic ligands have an important impact on the activities of the complexes.

2 | EXPERIMENTAL

2.1 | Materials and methods

The ligands HPBM and PBO were synthesized based on methods reported in the literature.[35,36] TBZ, Gl-L-Val, CT-DNA, ethidium bromide (EB), dimethylsulfoxide (DMSO), RPMI-1640 and DMEM were purchased from Sigma. pBR322 DNA was provided by MBI Fermentas (Lithuania). Cancer cell lines A549, PC-3 and HeLa and normal cell line 3 T3 were purchased from the American Type Culture Collection. MTT was obtained from Sinopharm Chemical Reagent Co. Ltd (Shanghai, China). All reagents and chemicals were of analytical reagent grade and were used as commercially purchased without any further purification.

DNA stock solution was prepared in buffer containing 5 mM Tris–HCl and 50 mM NaCl at pH = 7.2, and kept at 4 °C for no more than three days. The solution of CT-DNA gave a ratio of UV absorbance at 260 and 280 nm of about 1.8–1.9, indicating that the DNA was fully free of protein, and its concentration was determined by UV absorbance at 260 nm using an extinction coefficient of 6600 M^{-1} cm^{-1}.[37] Elemental analyses (C, H and N contents) were performed with a Vario EL elemental analyzer (Elementar, Germany). Fourier transfer infrared (FT-IR) spectra were recorded with samples as KBr pellets using a VERTEX 70 FT-TR spectrometer (Bruker, Germany) in the spectral range 400–4000 cm^{-1}. UV–visible, fluorescence, electrospray ionization (ESI) mass and electron spin resonance (ESR) spectra were obtained with a Pharmacia 2550 spectrophotometer (Shimadzu, Japan), Hitachi F-4500 fluorescence spectrophotometer (Hitachi, Japan), API4000 triple quadrupole mass spectrometer (AB Sciex, USA) and Bruker EMX A300 spectrometer (Bruker, Germany), respectively. The molar conductivities were measured using a DDS-11A digital conductance meter (LeiCi, Shanghai).

2.2 | Preparation of complexes

The complexes were prepared by a method similar to that reported in the literature.[34] $Cu(ClO_4)$·$6H_2O$ (0.5 mmol) aqueous solution was added into 5 ml of an aqueous solution containing Gly-L-Val (0.5 mmol) and NaOH (0.5 mmol) with stirring, and then HPBM/TBZ/PBO

(0.5 mmol) in 20 ml of CH_3OH was added dropwise into the mixture. The resultant solutions were stirred thoroughly, and the pH was adjusted to 4.83 with perchloric acid solution. These mixtures were further stirred for about 1 h at 50 °C and slowly evaporated to afford the complexes. The products were filtered, dried under vacuum and further purified by recrystallization from methanol–water (80% v/v).

Complex 1. Blue; yield: 70 %. Anal. Calcd for $C_{20}H_{28}N_5O_9ClCu$ (M_W = 582.91) (%): C, 41.31; H, 4.85; N, 12.05. Found (%): C, 41.23; H, 4.63; N, 11.98. FT-IR (KBr, cm^{-1}): ν(—OH) 3425; ν_{as}(—NH_2) 3104; ν_s(—NH_2) 2964; ν_{as}(—COO^-) 1615; ν_s(—COO^-) 1379; ν(C—N) 1458; ν(Cu—O) 621; ν(Cu—N) 433. UV–visible (MeOH; λ_{nm}/nm, ε/M^{-1} cm^{-1}): 323, 2.28 × 10^4; 666, 66.16.

Complex 2. Bluish-green; yield: 78 %. Anal. Calcd for $C_{17}H_{22}N_5O_8SClCu$ (M_W = 556.94) (%): C, 36.76; H, 3.99; N, 12.61. Found (%): C, 36.58; H, 4.17; N, 12.43. FT-IR (KBr, cm^{-1}): ν(—OH) 3409; ν_{as}(—NH_2) 3090; ν_s(—NH_2) 2962; ν_{as}(—COO^-) 1613; ν_s(—COO^-) 1326; ν(C—N) 1435; ν(Cu—O) 648; ν(Cu—N) 434. UV–visible (MeOH; λ_{nm}/nm, ε/M^{-1} cm^{-1}): 234, 2.88 × 10^4; 300, 3.68 × 10^4; 666, 87.45.

Complex 3. Blue; yield: 72 %. Anal. Calcd for $C_{19}H_{23}N_4O_9ClCu$ (M_W = 551.91) (%): C, 41.46; H, 4.21; N, 10.18. Found (%): C, 41.42; H, 4.01; N, 9.99. FT-IR (KBr, cm^{-1}): ν(—OH) 3422; ν_{as}(—NH_2) 3099; ν_s(—NH_2) 2962; ν_{as}(—COO^-) 1613; ν_s(—COO^-) 1376; ν(C—N) 1480; ν(Cu—O) 624; ν(Cu—N) 428. UV–visible (MeOH; λ_{nm}/nm, ε/M^{-1} cm^{-1}): 231, 1.41 × 10^4; 304, 2.65 × 10^4; 634, 60.07.

2.3 | Interaction with CT-DNA

2.3.1 | UV–visible absorption spectroscopy

Absorption spectra were determined in the range 210–500 nm by maintaining a constant complex concentration in the presence of CT-DNA for various *r* ([complex]/[CT-DNA] mixing ratio) values at room temperature. Meanwhile, the reference solution was used to remove the absorption of CT-DNA itself, and Tris buffer was subtracted through baseline correction. Every sample solution was permitted to equilibrate for 6 min before recording its spectrum.

2.3.2 | Fluorescence spectroscopy

Fluorescence quenching measurements were carried out at an excitation wavelength of 525 nm and emission wavelength set at 550–660 nm. The effect of the addition of each complex to a sample including EB and CT-DNA (8 and 10 μM, respectively) in Tris buffer (pH = 7.2) was investigated by recording the variation in fluorescence spectra.

2.3.3 | Viscosity measurements

Viscosity experiments were performed with an Ostwald viscometer immersed in a water bath maintained at 29 ± 0.1 °C for EB (standard) and complexes **1**, **2** and **3**. The concentration of CT-DNA was 200 μM, and the concentration of the complexes and EB was varied from 0 to 70 μM with 10 μM intervals. The flow time for every sample was determined three times with a digital stopwatch and then averaged. Relative viscosity values (η) were calculated based on the relation $\eta = (t - t_0)/t_0$, where t is the flow time of DNA-containing solutions and t_0 is the flow time of free buffer. The obtained data are presented as $(\eta/\eta_0)^{1/3}$ versus [complex]/[DNA], where η and η_0 are the viscosity of the CT-DNA solution in the absence and presence of the complexes, respectively.

2.3.4 | CD spectral measurements

CD spectra of CT-DNA (100 μM) with [complex]/[DNA] ratio of 0.6 were recorded from 220 to 320 nm using a 10 mm path quartz cuvette and a 100 nm min^{-1} scanning rate. Each spectrum was obtained by averaging three scans and subtracting the background signal of the buffer.

2.3.5 | Thermal denaturation studies

DNA thermal denaturation experiments were carried out with a Chirascan using CT-DNA (50 μM) by varying the temperature from 70 to 100 °C at a heating rate of 2 °C min^{-1}, both in the absence and presence of each complex (30 μM). The absorption changes at 260 nm were continuously monitored and the melting temperature (T_m) was defined as half of the total unbound base pairs, which was confirmed from the mid-point of the melting curves. The data were presented as $(A - A_1)/(A_f - A_1)$ versus temperature, where A, A_1 and A_f are the observed, initial and final absorbance, respectively.

2.3.6 | DNA excision measurements

Electrophoresis experiments were performed using pBR322 plasmid DNA according to established procedures. The samples were incubated at 37 °C for a period of 1 h in the dark. Then the reactions were quenched by addition of loading buffer and the analysis involved

loading of the solutions onto 0.8% agarose gels containing 5 μl of GoldView. The final solutions were subjected to gel electrophoresis (100 V for 40 min in standard Tris–boric acid–EDTA buffer, pH = 8.3). The gel bands obtained were visualized and photographed with a BIO-RAD Laboratories Segrate Gel Imaging System. Control experiments were carried out using 50 μM ascorbic acid (VC), 20 μM $Cu(ClO_4)_2{\cdot}6H_2O$ and 20 μM free ligands.

In order to explore the mechanism, the cleavage of supercoiled DNA was carried out in the presence of typical reactive oxygen species scavengers such as DMSO, ethanol and *tert*-butyl alcohol (hydroxyl radical), superoxide dismutase (SOD; superoxide anion radical) and sodium azide (singlet oxygen). Each sample was incubated at 37 °C for 1 h and analyzed according to the procedure described above.

2.3.7 | Molecular docking studies

The molecular docking studies were performed using the AutoDock Vina1.1.2 set of programs[38] with the Lamarckian genetic algorithm. The molecular structures of the complexes were sketched via Gaussian viewer, while the crystal structure of DNA d(5′-G-Diu-TGCAAC-3′) (PBD ID: 454D) was downloaded from the protein data bank. For docking, the water molecules and the substrate DNA were deleted, the active site was defined and selected, and a grid box was constructed to enclose the whole DNA molecule, setting the grid size to 60, 60, 60 with a spacing of 0.375 Å. Subsequently, the complexes were docked to the DNA under other default settings. Visualization of the docked conformation was produced with PyMol software.

2.4 | *In Vitro* cytotoxicity assays

The cytotoxic activities of the complexes and cisplatin were studied against cancer cell lines A549, PC-3 and HeLa and normal cell line 3 T3 using the MTT method, where cancer cell lines and normal cell line were cultured in RPMI-1640 and DMEM, respectively. All the cells were seeded into 96-well plates (1×10^4 per well) and cultured in a CO_2 incubator (37 °C, 5% CO_2). Once the cells adhered and reached 70–80% confluency, complex (3.125–200 μM) was added to each well, and incubated for 48 h. Then MTT reagent (20 μl, 5 mg ml^{-1}) was added. After 4 h, DMSO (100 μl) was added to solubilize the MTT formazan. Subsequently, the optical densities were measured at 490 nm with a microplate spectrophotometer. These data were obtained from triplicate independent cell passages and the IC_{50} values (drug concentration that inhibits cell growth by 50%) were calculated to evaluate the cytotoxic effects of the complexes.

2.5 | Antimicrobial studies

2.5.1 | Test microorganisms

The antimicrobial activities of the compounds (complexes and ligands) were determined against four strains of bacteria. Reference strains were Gram-positive bacteria *Bacillus subtilis* and *Staphylococcus aureus*, and Gram-negative bacteria *Escherichia coli* and *Pseudomonas aeruginosa*. These microorganisms were generously provided by the Key Laboratory of Plant Molecular Breeding of Guangdong Province, College of Agriculture, South China Agricultural University.

2.5.2 | Agar diffusion method

The antimicrobial activities of the prepared ligands and complexes were determined using the Oxford cup method. Each compound was dissolved at a concentration of 2 mg ml^{-1} in a mixed solvent of aseptic water with 5% DMSO. Under aseptic conditions Oxford cups were placed in inoculated agar media, and 100 μl of samples was inhaled into the cups. Then the agar plates were incubated for 24 h at 37 °C. After this period, the diameter of the inhibition zone formed around each cup was observed, and measured in millimeters. Each test was carried out in triplicate.

2.5.3 | Microdilution method

Screening was performed by determining the minimum inhibitory concentration (MIC) and the minimum bactericidal concentration (MBC) using the microdilution method with MTT.[39,40] The compounds were dissolved in sterile water containing 5% DMSO with concentrations of 1024, 800 and 640 μg ml^{-1}. Under twofold serial dilutions the concentration in the tubes was 512–1.00 μg ml^{-1} (400–1.81 and 320–1.25 μg ml^{-1}). Then, 10 μl of bacterial suspension (10^6 CFU ml^{-1}) was added to appropriate tubes. All cultures were incubated for 24 h in a shock incubator at 37 °C. Finally, 10 μl of phosphate-buffered saline including 5 mg ml^{-1} MTT, as an indicator of microbial growth, was added to each tube and incubated at 37 °C for 30 min. MTT is a light yellow dye that turns blue-violet when it is reduced to formazan by dehydrogenase within viable cells. The lowest concentrations of the test substances that prevented MTT color change from yellow to blue were considered as the MIC values. Then, 20 μl of each solution was extracted from the test tubes of the yellow solutions and coated on nutrient agar

medium. After 24 h incubation, the lowest concentration with no growth was defined as the MBC value. All the equipment and culture media were sterilized.

3 | RESULTS AND DISCUSSION

3.1 | Synthesis and spectroscopy

The complexes were synthesized in high yields (70–80%) via the reaction of equal molar ratio of Gly-L-Val with $Cu(ClO_4)_2{\cdot}6H_2O$ in the presence of HPBM/TBZ/PBO (Scheme 1). The structure of the complexes was confirmed using elemental analyses, molar conductivity measurements and various spectroscopies, namely FT-IR, UV–visible, ESI-MS and ESR. The results of elemental analyses corresponded with the theoretically expected values, which confirmed the compositions for all the complexes. The values of the molar conductivity of 1 mM MeOH solution of the three complexes are within the range 90–98 S cm^2 mol^{-1}, indicating 1:1 type electrolytes.[41] Furthermore, ESI-MS studies of the complexes were carried out in MeOH solution. The results showed peaks of mass-to-charge ratio m/z at 446.2, 437.1 and 432.0, which matched accurately with $[Cu(Gly\text{-}L\text{-}Val)(HPBM)]^+$, $[Cu(Gly\text{-}L\text{-}Val)(TBZ)]^+$ and $[Cu(Gly\text{-}L\text{-}Val)(PBO)]^+$, respectively.

The combining mode of Gly-L-Val was investigated using FT-IR spectroscopy. In the FT-IR spectra, the very broad peak at about 3420 cm^{-1} was assigned as ν(—OH) stretching vibration of the water molecules. The absorption peaks at 3104 and 2964 cm^{-1} for **1**, at 3090 and 2962 cm^{-1} for **2** and at 3099 and 2966 cm^{-1} for **3** were ascribed to the stretching vibrations ν_{as}(—NH_2) and ν_s(—NH_2), respectively, while the peaks at 1615 and 1379 cm^{-1} for **1**, 1613 and 1326 cm^{-1} for **2** and 1630 and 1376 cm^{-1} for **3** were assigned to ν_{as}(—COO^-) and ν_s(—COO^-) stretching vibrations of the carboxylate group of the coordinated dipeptide ligand, respectively. The $\Delta\nu$ (ν_{as}(—COO^-) − ν_s(—COO^-)) values in the range 236–287 cm^{-1} indicated the monodentate coordination mode of the carboxylate group of the dipeptide.[42] Moreover, the vibrations ν(C—N) and ν(C—C) were, respectively, at 1458 and 788 cm^{-1} for HPBM, at 1435 and 749 cm^{-1} for TBZ and at 1480 and 758 cm^{-1} for PBO, suggesting that HPBM/TBZ/PBO was coordinated to the central copper ion. Furthermore, the peaks at 433 and 621 cm^{-1} for **1**, 434 and 749 cm^{-1} for **2** and 428 and 624 cm^{-1} for **3** were assigned to the stretching vibrations ν(Cu—N) and ν(Cu—O), respectively. These overall characteristics of the FT-IR spectra further verified that the ligands were coordinated to the central copper(II) ion.[43–46]

The electronic spectra of the complexes in the UV–visible region were measured in methanol solution. The bands at 323 nm (ε = 22 766 M^{-1} cm^{-1}) for **1**, 234 nm (ε = 28 758 M^{-1} cm^{-1}) and 300 nm (ε = 36 769 M^{-1} cm^{-1}) for **2** and 231 nm (ε = 14 084 M^{-1} cm^{-1}) and 304 nm (ε = 26 460 M^{-1} cm^{-1}) for **3** were observed. These bands correspond to $\pi \rightarrow \pi^*$ transitions of ligand HPBM/TBZ/PBO. Furthermore, the broad and weak absorption bands observed in the range 634–666 nm (ε = 60–88 M^{-1} cm^{-1}) were attributed to the d → d transition of the copper(II) ion in a distorted square pyramidal environment.[47]

The X-band ESR spectra at 9.46 GHz were obtained using tetracyanoethylene as field marker under a magnetic field strength of 3000 ± 1000 gauss in MeOH (100 K). The optimal simulating parameters were obtained as follows: $g_{||}$ = 2.2618, $g_{\perp}$ = 2.0509 and $A_{||}$ = 157.120 for **1**, $g_{||}$ = 2.2585, $g_{\perp}$ = 2.0386 and $A_{||}$ = 155.843 for **2** and $g_{||}$ = 2.2865, $g_{\perp}$ = 2.0627 and $A_{||}$ = 165.777 for **3**. The order of $g_{||} > g_{\perp} > g_e$ (2.0023) showed that the unpaired electron in copper(II) was

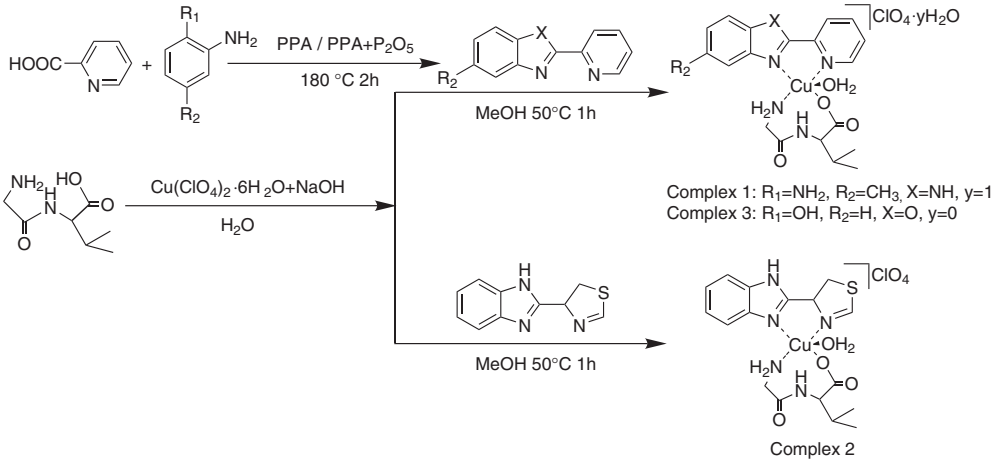

SCHEME 1 Synthesis of ligands and corresponding complexes

localized in the $d_{x^2-y^2}$ orbital, revealing the nearly square pyramidal coordination geometry of the copper(II) ion.[48,49]

Therefore, based on the above experimental results and relevant literature,[32–34] the preliminary structures of the three copper(II) complexes could be proposed with an approximate square pyramidal geometry in which four equatorial positions were occupied by Gly-L-Val (N, O) and aromatic heterocycle (N, N) and the axial position was occupied by an O atom of H_2O as shown in Scheme 1.

3.2 | Interaction with CT-DNA

3.2.1 | Electronic absorption spectra

Electronic absorption spectroscopy is an effective method for investigating the binding pattern and strength of metal complexes with DNA. As the intercalative mode involves a stacking interaction between the aromatic chromophore of a complex and the base pairs of DNA, hypochromism and red-shift are usually associated with the insertion ability of complexes to DNA.[50] The absorption spectra of complexes **1**–**3** with DNA were recorded for a constant complex concentration (5.0×10^{-5} M) with various [complex]/[DNA] ratios (r). Representative spectra of the complexes with DNA derived for various mixing ratios are shown in Figure 1. The intensity of the absorption bands was gradually decreased, with maximum hypochromism of 40.35, 22.39 and 11.94%, respectively, for complexes **1**, **2** and **3**. In order to compare the DNA binding affinities of **1**–**3** quantitatively, the binding constants (K_b) were calculated using the following equation:[51]

$$\frac{[\mathrm{DNA}]}{\varepsilon_a - \varepsilon_f} = \frac{[\mathrm{DNA}]}{\varepsilon_b - \varepsilon_f} + \frac{1}{K_b(\varepsilon_b - \varepsilon_f)} \quad (1)$$

in which [DNA] is the concentration of DNA and ε_a, ε_b and ε_f denote, respectively, A_{obs}/C_{Cu}, extinction coefficients of complex in bound form and free. Also, the ratio of slope to intercept was obtained in a plot of [DNA]/($\varepsilon_a - \varepsilon_f$) versus [DNA]. The obtained K_b values for complexes **1**, **2** and **3** were 3.78×10^5, 7.47×10^4 and 2.28×10^4 M^{-1}, respectively, following the order **1** > **2** > **3**. The K_b values showed that **1** and **2** exhibit stronger DNA binding ability than **3**, which may be because the NH group on the imidazole ring of HPBM and TBZ can more easily form hydrogen bonds than the O atom on the thiazole ring of PBO, which was verified by the molecular docking studies (Section 3.2.7). In addition, the DNA binding ability of **1** was significantly stronger than that of **2**, which was due to HPBM with large planarity and high lipophilicity.

3.2.2 | Fluorescence spectra

To further confirm the binding mode of the complexes with DNA, competitive binding experiments using EB as a probe were carried out (Figure 2). The DNA–EB fluorescence intensity decreased on addition of the complexes, showing that the complexes could displace EB from the DNA–EB system and interact with DNA through an intercalative mode.[52] Additionally, the Stern–Volmer constant quenching constants (K_{sv}), a measure of the binding propensity of complexes to DNA, were calculated using the following equation:[53]

$$\frac{I_0}{I} = 1 + K_{sv}[\mathrm{Q}] \quad (2)$$

in which I_0 and I are the fluorescence intensities of DNA + EB in the absence and presence of quencher, respectively, K_{sv} is the Sterm–Volmer quenching constant and [Q] is the concentration of the quencher. The K_{sv} values of the complexes at 300 K were obtained as 1.774×10^4, 1.532×10^4 and 4.350×10^3 M^{-1}, respectively, following the order **1** > **2** > **3**, which was consistent with the electronic absorption spectroscopy results.

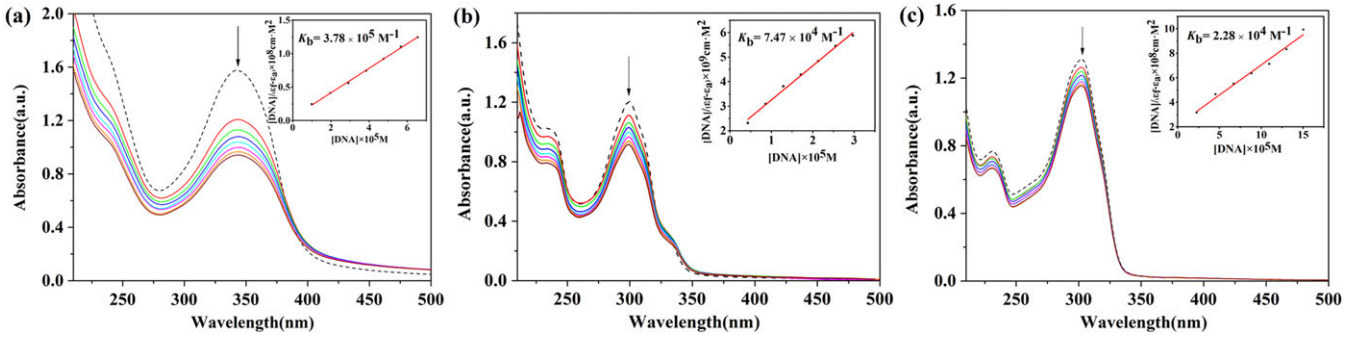

FIGURE 1 Absorption spectra of complexes (a) **1**, (b) **2** and (c) **3**. Arrows indicate the change upon increasing DNA concentration. Insets: Plots of [DNA]/($\varepsilon_f - \varepsilon_a$) versus [DNA] for the titration of DNA with complexes

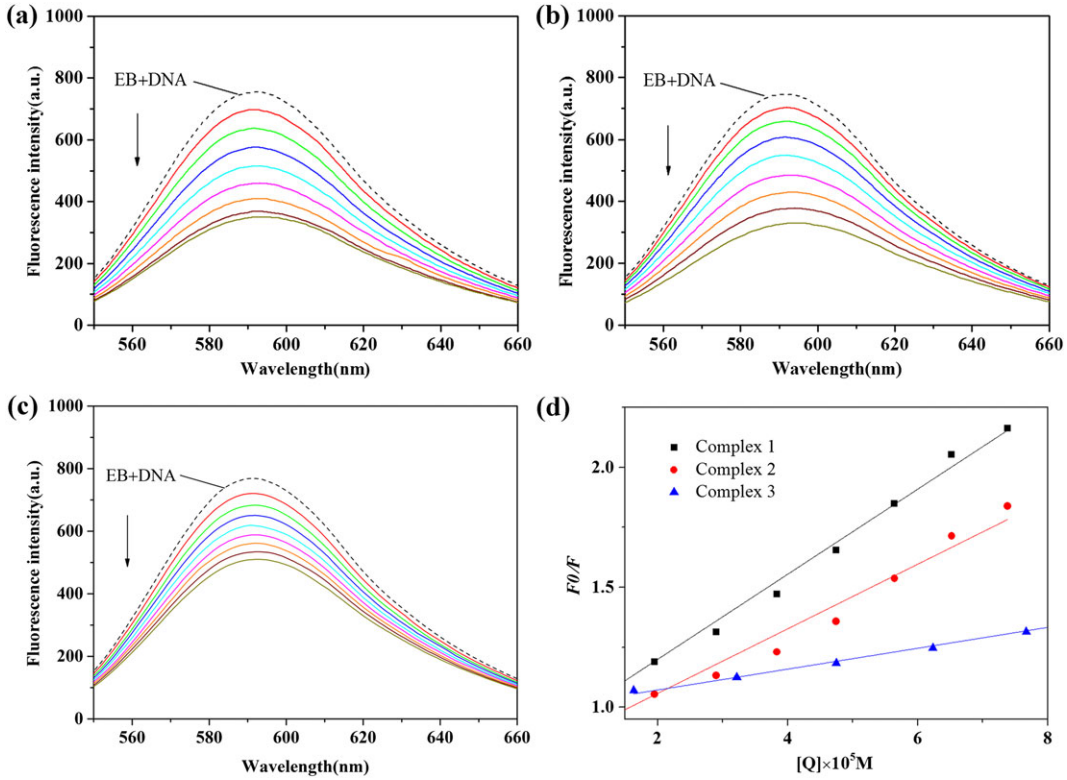

FIGURE 2 Emission spectra of CT DNA–EB system upon titration of complexes (a) **1**, (b) **2** and (c) **3**. The arrows show the change upon increasing concentration of complexes. (d) Plot of F_0/F versus [Q] for the titration of the complexes

3.2.3 | Viscosity measurements

The viscosity of DNA, which is sensitive enough to DNA length changes, can offer reliable evidence for the interactive binding mode of complexes with DNA. If the interaction mode is intercalative, DNA base pairs will separate to contain the bound compound, resulting in an increase of the DNA helix length, and thus an increase in DNA viscosity. On the other hand, if a complex binds to DNA by a partial or non-classic intercalative mode, DNA helix will bend or kink, thus causing a reduction of its valid length, with the DNA viscosity keeping invariant or displaying a slight decrease.[54–56] In order to further illustrate the essence of the interaction between the complexes and DNA, viscosity measurements were performed and the results are shown in Figure 3. The relative viscosity of DNA increased continuously with the addition of the complexes, indicating that the complexes bind to DNA through an intercalative mode. The increased degree of the viscosity follows the order **1** > **2** > **3**, which was in agreement with the results obtained from electronic absorption spectra and fluorescence spectra.

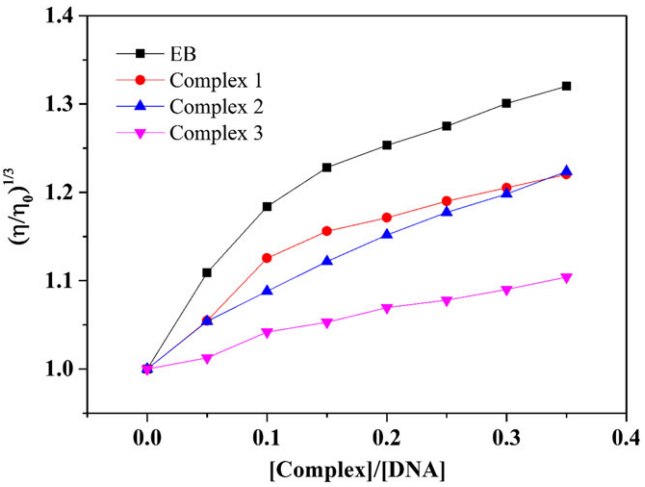

FIGURE 3 Relative viscosities of CT-DNA (50 μM) in the presence of the complexes and EB at 302 K

3.2.4 | CD spectra

The technique of CD spectroscopy is quite sensitive to DNA conformation changes which are caused by small molecule–DNA interactions, so we can monitor these very smalls DNA changes by using this technique and then obtain useful conformation information. The CD spectrum of free DNA consists of two CD signals: a positive band due to base stacking (274 nm) and a negative one due to right-hand helicity (246 nm) of B-DNA, while changes in these signals are usually ascribed to corresponding changes in DNA structure.[22,57,58] The

CD spectra of DNA with complexes **1**–**3** are shown in Figure 4. On addition of the complexes to DNA solution, the strength of the DNA bands was decreased and the strength of the positive band was obviously higher than that of the negative band. This phenomenon is generally observed when a complex is intercalated into the bases of DNA, since it unwinds the double helix of DNA, and thus decreases the strength of the CD bands.[59] The results showed that the decreasing extent of these bands kept the order **1** > **2** > **3**, which was in accordance with the binding abilities of the complexes to DNA.

3.2.5 | DNA thermal denaturation

DNA melting experiment is an important tool for studying the interaction of small molecules with DNA. A melting temperature (T_m) change of about 5–8 °C is usually observed upon the intercalation of complexes into DNA, whereas non-intercalation of complexes leads to no marked increase in melting point.[58] Under our experimental conditions, the melting curves of DNA in the absence and presence of complexes **1**–**3** are provided in Figure 5. The T_m of DNA was 84.5 °C and that in the presence of complexes **1**, **2** and **3** was 91.6, 91.1 and 88.9 °C, respectively. Therefore, the ΔT_m values (7.1, 6.6 and 4.4 °C) indicated that complexes **1** and **2** could be strongly inserted into DNA, but complex **3** could only be slightly inserted. Moreover, the ΔT_m changes revealed the bonding strength still follows the order of **1** > **2** > **3**, which was consistent with the results of studies discussed above.

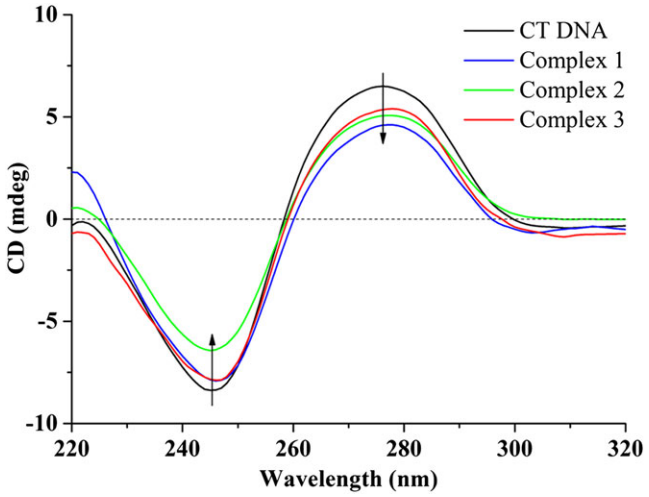

FIGURE 4 CD spectra of complexes **1**, **2** and **3** upon titration of CT-DNA at a molar ratio of 3:5 (complex to DNA)

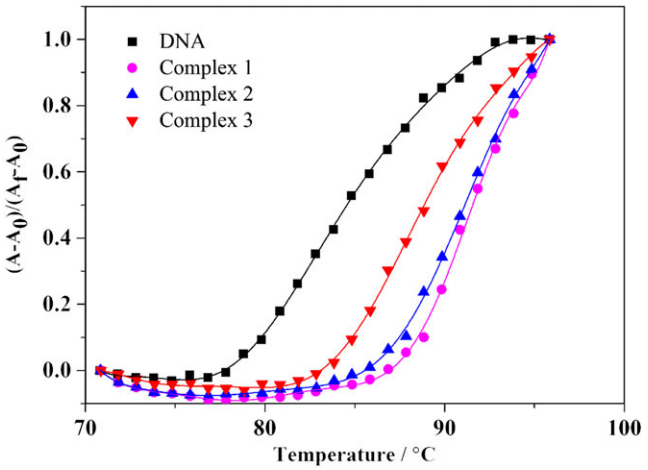

FIGURE 5 Temperature melting curves of CT-DNA (50 μM) in the absence and presence of complexes (30 μM) at 260 nm

3.2.6 | pBR322 DNA excision

The DNA cleavage ability of complexes **1**–**3** was monitored using the agarose gel electrophoresis technique by reacting supercoiled pBR322 plasmid DNA (20 μM) with **1**–**3** (5, 10, 15 and 20 μM) in the absence and presence of VC (50 μM) (Figure 6; Table 1). When DNA alone, VC, $Cu(ClO_4)\cdot 6H_2O$, HPBM/TBZ/PBO, Gly-L-Val and complexes **1**–**3** were used for control experiment, no marked cleavage was observed, but the complexes could cleave DNA more efficiently in the presence of VC, and the cleavage exhibited a concentration-dependent manner. Among the complexes, **1** possessed the highest DNA cleavage activity (Table 1), which was closely linked to its highest DNA binding affinity (as discussed above).

In order to investigate the DNA cleavage mechanism of the complexes, various additives, namely hydroxyl radical scavengers (DMSO, *tert*-butyl alcohol and EtOH), a singlet oxygen scavenger (NaN_3) and a superoxide anion scavenger (SOD), were used to determine the nature of the reactive species involved in the DNA oxidative cleavage reactions (Figure 7; Table 2). When a hydroxyl radical scavenger (DMSO, *tert*-butyl alcohol and EtOH) was added to the reaction mixture of the complexes and pBR322 DNA, the DNA cleavage activity was significantly inhibited (lanes 4–6), suggesting the involvement of $^{\bullet}OH$ radicals in the DNA cleavage process. Upon adding a singlet oxygen ($^1O_2$) quencher (NaN_3) to the reaction mixture, the cleavage activity was not clearly inhibited (lane 7), indicating that $^1O_2$ was not involved in the cleavage process. Furthermore, upon addition of superoxide anion scavenger (SOD) to the reaction mixture, cleavage reactions were promoted (lane 8), revealing that $O_2^{\bullet -}$ was likely to be indirectly involved in the cleavage process.

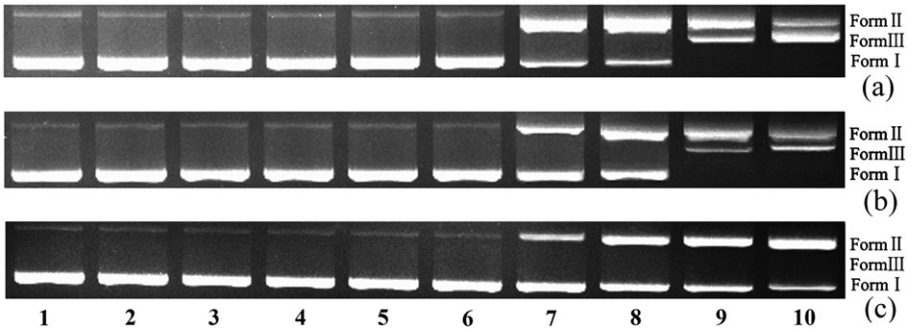

FIGURE 6 Cleavage of pBR322 DNA (250 ng) with (a) **1**, (b) **2** and (c) **3**. Lane 1, DNA control; lane 2, DNA + VC (50 μM); lane 3, DNA + $Cu(ClO_4)\cdot 6H_2O$ (20 μM); lane 4, DNA + HPBM/TBZ/PBO (20 μM); lane 5, DNA + Gly-L-Val (20 μM); lane 6, DNA + **1**/**2**/**3** (20 μM); lanes 7–10, DNA + VC (50 μM) + **1**/**2**/**3** (5, 10, 15 and 20 μM, respectively)

TABLE 1 Cleavage of pBR322 DNA by complexes after incubation for 1 h at 37 °C

		Form (%)		
Lane number	**Reaction conditions**	**I**	**II**	**III**
1	DNA (**1**/**2**/**3**)	88.4/91.2/94.9	11.6/8.8/5.1	0/0/0
6	DNA + **1**/**2**/**3** (20 μM)	88.1/90.0/92.0	11.9/10.0/8.0	0/0/0
7	DNA + VC + **1**/**2**/**3** (5 μM)	33.5/61.5/74.4	66.5/38.5/25.6	0/0/0
8	DNA + VC + **1**/**2**/**3** (10 μM)	27.1/46.4/49.7	72.9/53.6/50.3	0/0/0
9	DNA + VC + **1**/**2**/**3** (15 μM)	0/0/39.3	68.1/82.7/60.7	31.9/17.3/0
10	DNA + VC + **1**/**2**/**3** (20 μM)	0/0/21.2	28.6/40.6/78.8	71.4/59.4/0

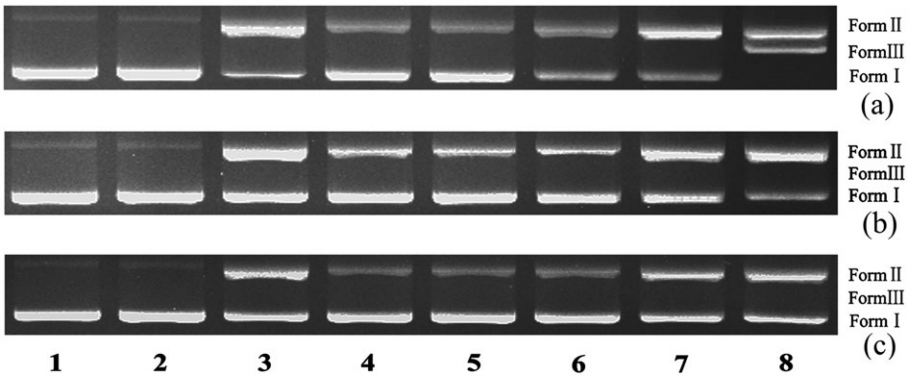

FIGURE 7 Cleavage of pBR322 DNA (250 ng) by (a) **1**, (b) **2** and (c) **3** at 37 °C with incubation time of 1 h in the presence of various typical reactive oxygen species scavengers. Lane 1, DNA control; lane 2, DNA + VC (50 μM) + SOD (15 units); lane 3, DNA + VC (50 μM) + **1**/**2**/**3** (10 μM); lanes 4–8, DNA + VC (50 μM) + **1**/**2**/**3** (10 μM) + [DMSO (0.2 M), *tert*-butyl alcohol (0.2 M), EtOH (0.2 M), NaN_3 (0.2 M) and SOD (15 units), respectively]

All the results suggested that the complexes oxidatively cleaved DNA through the $^{\bullet}OH$ mechanism.

3.2.7 | Molecular docking

The molecular docking technique, as a tool to assist in biophysics research, can simulate the binding of biomolecules like DNA towards small molecules or drug molecules with the aid of a computer.[58,60] For the purpose of this work, we chose double-strand DNA with the sequence d(5′-G-dIU-TGCAAC-3′) (PDB ID: 454D). The results of analyses of docking between the complexes and DNA are shown in Figure 8. The resulting docked models indicated that complexes **1**–**3** were likely to insert

TABLE 2 Oxidative cleavage of pBR322 DNA by complexes in presence of various typical reactive oxygen species scavengers after incubation for 1 h at 37 °C

Lane number	Reaction conditions	Form (%)		
		I	II	III
1	DNA (**1**/**2**/**3**)	90.7/87.8/92.7	9.3/12.3/7.3	0/0/0
3	DNA + VC + **1**/**2**/**3**	24.5/48.2/52.2	75.5/51.8/47.8	0/0/0
4	DNA + VC + **1**/**2**/**3** + DMSO	69.9/64.4/77.0	30.1/35.6/23.0	0/0/0
5	DNA + VC + **1**/**2**/**3** + *tert*-butyl alcohol	71.3/65.3/75.8	28.7/34.7/24.2	0/0/0
6	DNA + VC + **1**/**2**/**3** + EtOH	61.4/68.8/70.2	38.6/31.2/29.8	0/0/0
7	DNA + VC + **1**/**2**/**3** + NaN_3	30.4/45.1/48.2	69.6/54.9/51.8	0/0/0
8	DNA + VC + **1**/**2**/**3** + SOD	0/23.9/38.4	55.3/76.1/61.6	44.7/0/0

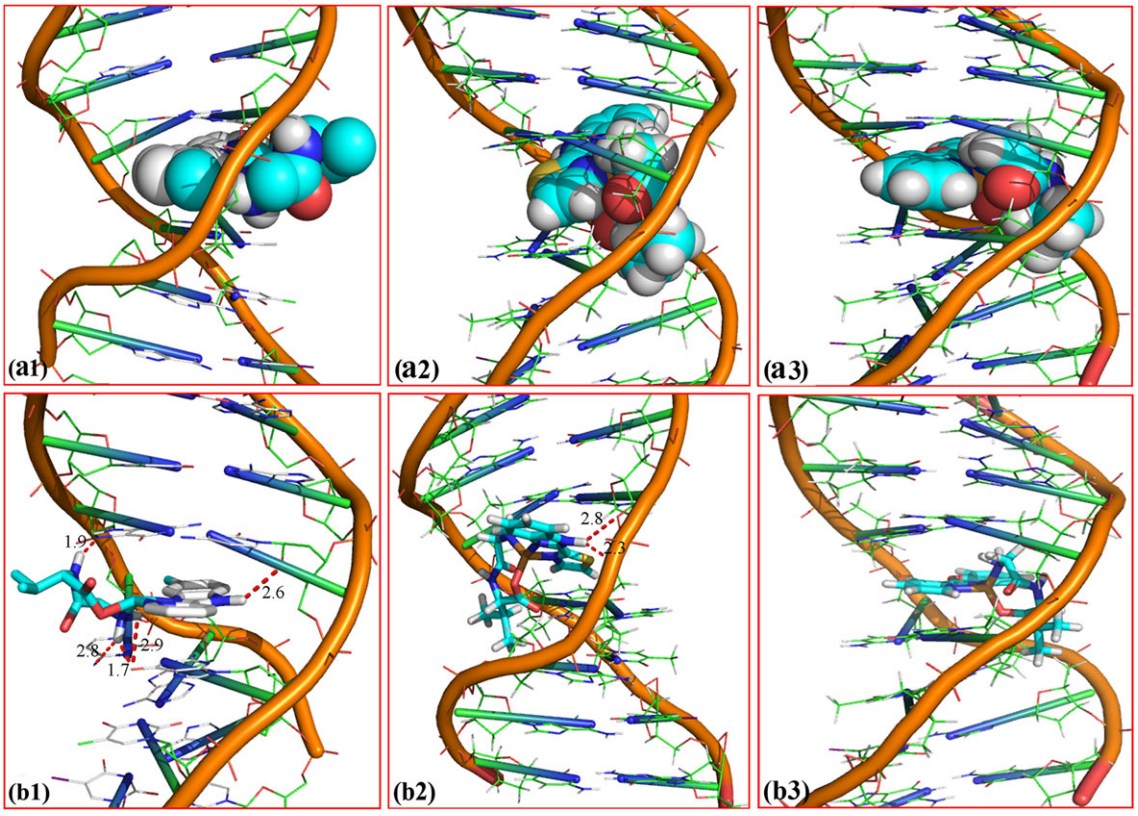

FIGURE 8 Molecular docked models of (a) complexes (spheres representation) with DNA. (b) Hydrogen bonds of the complexes (stick representation) and DNA (cartoon form) are expressed as red dashed lines. (a1, b1: Complex **1**; a2, b2: Complex **2**; a3, b3: Complex **3**)

into the empty cavity within GC/GC base pair-rich region from the DNA central position through the aromatic heterocyclic ligands. Thus, hydrophobic interactions were the main force. Moreover, different amounts of hydrogen bonds were formed between the complexes and DNA. The hydrogen-bonding interaction had an important effect on the binding affinity of the complexes with DNA, in which complex **1** showed the best binding affinity due to it forming more hydrogen bonds with DNA nucleobases G4, G12, C5 and C13, but complex **3** had the lowest binding affinity owing to a lack of interaction. The resulting relative binding energies of the docked complexes **1**–**3** with DNA were found to be −37.24, −32.46 and −30.06 kJ mol^{-1}, respectively. The more negative the relative binding energy, the stronger the binding ability of the complex to DNA. Therefore, the docking results revealed that the binding affinities of the complexes with DNA followed the order **1** > **2** > **3**, which was positively related to the experimental results of DNA binding discussed above.

3.3 | *In Vitro* cytotoxicity

The cytotoxic activity of the complexes against cell lines A549, PC-3, HeLa and 3 T3 was studied by using the MTT method with cisplatin as a positive control. All cell lines were incubated for 48 h with an increasing concentration (3.125–200 μM) of each of **1**, **2** and **3**. The results were analyzed by cell inhibition expressed as IC_{50} values (Table 3). The results showed that the order of cytotoxicity was **1** > cisplatin > **2** > **3**, which was in good agreement with their DNA binding and oxidative DNA cleavage abilities. The copper complex with HPBM was more active than that with TBZ/PBO, which may be due to the higher lipid solubility of HPBM. However, **1** exhibited higher cytotoxic effects against the normal cell line (3 T3) than tumor cell lines (HeLa, A549 and PC-3). In addition, compared with the results of our previous research,[28] it was found that the copper(II) complexes with Gly-L-Val were more cytotoxic than those with Gly-gly, and the influence of N,N-aromatic heterocyclic ligands was more noticeable than that of dipeptides.

Of note, complex **2** exhibited lower cytotoxic effect compared with cisplatin, but it had no injurious effect on normal cells, indicating that **2** might be suitable as an effective anticancer drug against PC-3.

3.4 | *In Vitro* antibacterial activity

In order to explore the antibacterial properties of the complexes, $Cu(ClO_4)_2{\cdot}6H_2O$, Gly-L-Val, HPBM, TBZ, PBO and complexes **1**, **2** and **3** were evaluated against microorganisms *B. subtilis*, *S. aureus*, *E. coli* and *P. aeruginosa* through the agar diffusion and double dilution methods.

The diameters of inhibition zones as well as the MIC and MBC values are presented in Figure 9 and Tables 4 and 5. From Figure 9, it can be seen that both the complexes and some ligands showed certain inhibition for all bacterial strains, but TBZ ligand did not show any inhibition. The sensitivity rank of the complexes against

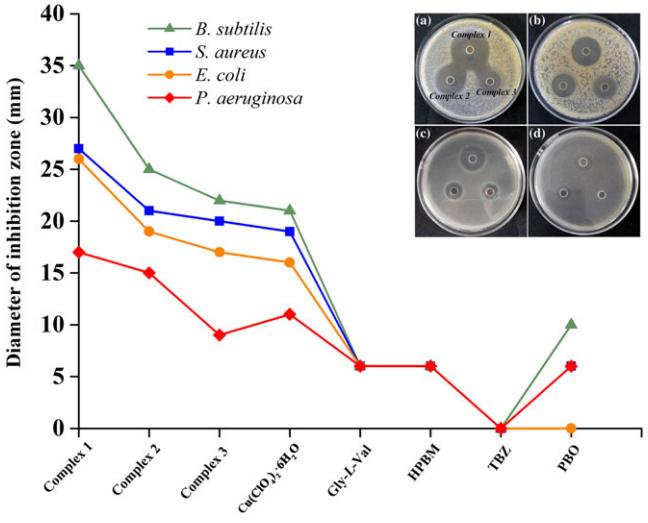

FIGURE 9 Antibacterial activities of the complexes, $Cu(ClO_4)_2{\cdot}6H_2O$, Gly-L-Val, HPBM, TBZ and PBO against *B. subtilis*, *S. aureus*, *E.coli* and *P. aeruginosa*. Inset: (a) *B. subtilis*; (b) *S. aureus*; (c) *E.coli*; (d) *P. aeruginosa*

the microorganisms was *B. subtilis* > *S. aureus* > *E. coli* > *P. aeruginosa*. The complexes showed higher antimicrobial activities than the corresponding ligands, which might be mainly due to the structural changes caused by coordination. In the complexes, the polarity of the metal ion was reduced due to the partial sharing of the negative charge of the heterocyclic ligands, thereby causing an increase of the lipophilic nature of the central metal ion which could penetrate into lipid layers of microorganisms more efficiently and then destroy them.

The higher antimicrobial activities of **1** and **2** compared with **3** may be attributed to the better biocompatibility of the benzimidazole-like ligands.[18,20] The antimicrobial activity of complex **1** was significantly greater than that of complex **2**, which may be mainly due to the relatively strong lipophilic property of HPBM compared with TBZ, having been verified by experiment. Furthermore, the results using the dilution method also proved the above results of the agar diffusion method. It

TABLE 3 IC_{50} values of complexes and cisplatin against various cell lines

	IC_{50} (μM)			
Compound	**A549**	**PC-3**	**HeLa**	**3 T3**
Complex **1**	10.08 ± 0.3	13.09 ± 0.7	9.93 ± 0.3	9.33 ± 0.5
Complex **2**	61.73 ± 3.7	38.04 ± 1.8	56.84 ± 5.6	138.04 ± 1.4
Complex **3**	66.10 ± 2.6	101.93 ± 11.2	81.02 ± 9.5	83.18 ± 2.0
Cisplatin	24.77 ± 1.7	20.93 ± 1.4	17.39 ± 3.7	29.51 ± 1.9
$[Cu(PBO)(Gly\text{-}gly)(H_2O)]{\cdot}ClO_4{\cdot}1.5H_2O$[24]	68.14 ± 1.8	93.44 ± 5.8	98.63 ± 6.9	—

TABLE 4 Antibacterial activities (μg ml^{-1}) of complexes and $Cu(ClO_4)_2{\cdot}6H_2O$

	Complex 1		Complex 2		Complex 3		$Cu(ClO_4)_2{\cdot}6H_2O$	
Species	**MIC**	**MBC**	**MIC**	**MBC**	**MIC**	**MBC**	**MIC**	**MBC**
B. subtilis	13	16	100	128	150	160	300	320
S. aureus	18	20	150	320	320	320	320	400
E. coli	26	32	200	256	320	512	320	512
P. aeruginosa	64	512	320	>512	400	>512	512	>512

TABLE 5 Antibacterial activities (μg ml^{-1}) of ligands (HPBM, TBZ, PBO, Gly-L-Val)

	HPBM		TBZ		PBO		Gly-L-Val	
Species	**MIC**	**MBC**	**MIC**	**MBC**	**MIC**	**MBC**	**MIC**	**MBC**
B. Subtilis	64	512	320	>512	>512	>512	>512	>512
S. Aureus	320	>512	>512	>512	>512	>512	>512	>512
E. Coli	64	>512	400	>512	>512	>512	>512	>512
P. Aeruginosa	512	>512	512	>512	>512	>512	>512	>512

is evident (Table 4) that the antimicrobial activity of complex **1** is much greater than that of the other two complexes, indicating that the complex has more potential for clinical application.

4 | CONCLUSIONS

Three new copper(II) complexes containing Gly-L-Val and N,N-aromatic heterocyclic ligand were synthesized and characterized. DNA binding, DNA cleavage, cytotoxicity and antibacterial activities were investigated. The interaction of the complexes with CT-DNA has been studied with various spectroscopic techniques, and it has been revealed that the complexes bind to CT-DNA through the intercalative mode. In subsequent experiments, pBR322 DNA cleavage verified that the complexes could induce DNA damage in the presence of VC. The cytotoxicity of the complexes was investigated against three different cancer cell lines (A549, PC-3 and HeLa) and normal cell line (3 T3). The IC_{50} values indicated that complex **1** exhibited high cytotoxicity. In addition, the cytotoxic effect of **2** was lower than that of **1** and cisplatin, but it has no injurious effect on normal cell line, indicating that **2** has the potential as an effective anticancer drug against PC-3. Furthermore, the antibacterial activity of the complexes against four different microorganisms was enhanced compared with the free ligands, and the structures of the N,N-aromatic heterocyclic ligands influenced the activity in the order of HPBM > TBZ > PBO. These encouraging studies may provide valuable insights into the rational design of potential novel antitumor and antibacterial agents in the future.

ACKNOWLEDGMENTS

This work was supported by the Natural Science Fund (no. 2015A030313423) and College Students' Innovation and Entrepreneurship Training Program (no. 1056413042) in Guangdong.

ORCID

Xue-Yi Le http://orcid.org/0000-0002-5703-336X

REFERENCES

[1] C. H. Leung, H. Z. He, L. J. Liu, M. Wang, S. H. Chan, D. L. Ma, *Coord. Chem. Rev.* **2013**, *257*, 3139.

[2] U. Ndagi, N. Mhlongo, M. E. Soliman, *Drug Des. Dev. Ther.* **2017**, *11*, 599.

[3] C. Santini, M. Pellei, V. Gandin, M. Porchia, F. Tisato, C. Marzano, *Chem. Rev.* **2014**, *114*, 815.

[4] K. M. Deo, B. J. Pages, D. L. Ang, C. P. Gordon, J. R. Aldrich-Wright, *Int. J. Mol. Sci.* **2016**, *17*, 1818.

[5] K. H. Reddy, *J. Indian Chem. Soc.* **2003**, *80*, 69.

[6] A. T. Chaviara, P. C. Christidis, A. Papageorgiou, E. Chrysogelou, D. J. Hadjipavlou-Litina, C. A. Bolos, *J. Inorg. Biochem.* **2005**, *99*, 2102.

[7] A. Meenongwa, R. F. Brissos, C. Soikum, P. Chaveerach, P. Gamez, Y. Trongpaniche, U. Chaveerach, *New J. Chem.* **2016**, *40*, 5861.

[8] A. Jayamani, V. Thamilarasan, N. Sengottuvelan, P. Manisankar, S. K. Kang, Y. I. Kim, V. Ganesan, *Spectrochim. Acta A* **2014**, *122*, 365.

[9] T. Kiran, V. G. Prasanth, M. M. Balamurali, C. S. Vasavi, P. Munusami, K. I. Sathiyanarayanan, M. Pathak, *Inorg. Chim. Acta* **2015**, *433*, 26.

[10] R. A. Steiner, D. Foreman, H. X. Lin, B. K. Carney, K. M. Fox, L. Cassimeris, J. M. Tanski, L. A. Tyler, *J. Inorg. Biochem.* **2014**, *137*, 1.

[11] M. J. Li, T. Y. Lan, X. H. Cao, H. H. Yang, Y. P. Shi, C. Q. Yi, G. N. Chen, *Dalton Trans.* **2014**, *43*, 2789.

[12] B. L. Fei, W. S. Xu, H. W. Tao, W. Li, Y. Zhang, J. Y. Long, Q. B. Liu, B. Xia, W. Y. Sun, *J. Photochem. Photobiol. B* **2014**, *132*, 36.

[13] R. Kumar, S. Obrai, A. Kaur, G. Hundal, H. Meehnian, A. K. Jana, *Polyhedron* **2013**, *56*, 55.

[14] R. Kumar, S. Obrai, A. Kaur, M. S. Hundal, J. Mitra, S. Sharma, *J. Coord. Chem.* **2015**, *68*, 2130.

[15] R. Kumar, S. Obrai, A. Sharma, A. K. Jassal, M. S. Hundal, J. Mitra, *J. Mol. Struct.* **2014**, *1075*, 43.

[16] P. Singla, V. Luxami, R. Singh, V. Tandon, K. Paul, *Eur. J. Med. Chem.* **2017**, *126*, 24.

[17] P. Vicini, M. Incerti, L. Amoretti, V. Ballabeni, M. Tognolini, E. Barocelli, *Farmaco* **2002**, *57*, 363.

[18] H. Z. Zhang, S. C. He, Y. J. Peng, H. J. Zhang, L. Gopala, V. K. R. Tangadanchu, L. L. Gan, C. H. Zhou, *Eur. J. Med. Chem.* **2017**, *136*, 165.

[19] J. Akhtar, A. A. Khan, Z. Ali, R. Haider, M. S. Yar, *Eur. J. Med. Chem.* **2017**, *125*, 143.

[20] N. Shrivastava, M. J. Naim, M. J. Alam, F. Nawaz, S. Ahmed, O. Alam, *Arch. Pharm.* **2017**, *350*, e201700040.

[21] J. Y. Hu, C. L. Liao, Y. Guo, F. Yang, W. Sang, J. A. Zhao, *Polyhedron* **2017**, *132*, 28.

[22] A. Saswati, S. Chakraborty, P. Dash, A. K. Panda, R. Acharyya, A. Biswas, S. Mukhopadhyay, S. K. Bhutia, A. Crochet, Y. P. Patil, M. Nethajie, R. Dinda, *Dalton Trans.* **2015**, *44*, 6140.

[23] S. Mandal, G. Das, H. Askari, *New J. Chem.* **2015**, *39*, 5208.

[24] M. Yagasaki, S. I. Hashimoto, *Appl. Microbiol. Biotechnol.* **2008**, *81*, 13.

[25] G. Facchin, M. H. Torre, E. Kremer, O. E. Piro, E. E. Castellano, E. J. Baran, *J. Inorg. Biochem.* **2002**, *89*, 174.

[26] R. Pogni, M. C. Baratto, E. Busi, R. Basosi, *J. Inorg. Biochem.* **1999**, *73*, 157.

[27] S. Iglesias, N. Alvarez, M. H. Torre, E. Kremer, J. Ellena, R. R. Ribeiro, R. P. Barroso, A. J. Costa-Filho, M. G. Kramer, G. Facchin, *J. Inorg. Biochem.* **2014**, *139*, 117.

[28] X. B. Fu, D. D. Liu, Y. Lin, W. Hu, Z. W. Mao, X. Y. Le, *Dalton Trans.* **2014**, *43*, 8721.

[29] X. B. Fu, J. J. Zhang, D. D. Liu, Q. Gan, H. W. Gao, Z. W. Mao, X. Y. Le, *J. Inorg. Biochem.* **2015**, *143*, 77.

[30] X. B. Fu, Z. H. Lin, H. F. Liu, X. Y. Le, *Spectrochim. Acta A* **2014**, *122*, 22.

[31] X. B. Fu, G. T. Weng, D. D. Liu, X. Y. Le, *J. Photochem. Photobiol. A* **2014**, *276*, 83.

[32] Q. Gan, Y. Y. Qi, Y. H. Xiong, Y. L. Fu, X. Y. Le, *J. Fluoresc.* **2017**, *27*, 701.

[33] Q. Gan, X. B. Fu, W. J. Chen, Y. H. Xiong, Y. L. Fu, S. Chen, X. Y. Le, *J. Fluoresc.* **2016**, *26*, 905.

[34] Q. Gan, C. L. Zhang, B. F. Wang, Y. H. Xiong, Y. L. Fu, Z. W. Mao, X. Y. Le, *RSC Adv.* **2016**, *6*, 35952.

[35] R. Schiffmann, A. Neugebauer, C. D. Klein, *J. Med. Chem.* **2006**, *49*, 511.

[36] A. W. Addison, T. N. Rao, C. G. Wahlgen, *J. Heterocycl. Chem.* **1983**, *20*, 1481.

[37] M. E. Reichmann, S. A. Rice, C. A. Thomas, P. Doty, *J. Am. Chem. Soc.* **1954**, *76*, 3047.

[38] O. Trott, A. J. Olson, *J. Comput. Chem.* **2010**, *31*, 455.

[39] A. M. Bukonjic, D. L. Tomovic, M. V. Nikolic, M. Z. Mijajlovic, V. V. Jevtic, Z. R. Ratkovic, S. B. Novakovic, G. A. Bogdanovic, I. D. Radojevic, J. Z. Maksimovic, S. M. Vasic, L. R. Comic, S. R. Trifunovic, G. P. Radic, *J. Mol. Struct.* **2017**, *1128*, 330.

[40] S. Indoria, T. S. Lobana, H. Sood, D. S. Arora, G. Hundal, J. P. Jasinski, *New J. Chem.* **2016**, *40*, 3642.

[41] W. J. Geary, *Coord. Chem. Rev.* **1971**, *7*, 81.

[42] K. Nakamoto, *Appl. Inorg. Chem.* **2008**, *77*, 1122.

[43] R. S. Kumar, S. Arunachalam, *Eur. J. Med. Chem.* **2009**, *44*, 1878.

[44] A. Garcıa-Raso, J. J. Fiol, B. Adrover, V. Moreno, I. Mata, E. Espinosa, E. Molins, *J. Inorg. Biochem.* **2003**, *95*, 77.

[45] P. R. Reddy, N. Raju, *Polyhedron* **2012**, *44*, 1.

[46] F. Arjmand, A. Jamsheera, D. K. Mohapatra, *J. Photochem. Photobiol. B* **2013**, *121*, 75.

[47] E. Prenesti, P. G. Daniele, S. Berto, S. Toso, *Polyhedron* **2006**, *25*, 2815.

[48] S. K. Tadavi, J. D. Rajput, S. D. Bagul, A. A. Hosamani, J. N. Sangshetti, R. S. Bendre, *Res. Chem. Intermed.* **2017**, *43*, 4863.

[49] B. Annaraj, M. A. Neelakantan, *Eur. J. Med. Chem.* **2015**, *102*, 1.

[50] G. W. Zhang, P. Fu, L. Wang, M. M. Hu, *J. Agric. Food Chem.* **2011**, *59*, 8944.

[51] P. Sinha, N. Kumari, K. Singh, K. Singh, L. Mishra, *Inorg. Chim. Acta* **2015**, *432*, 71.

[52] S. Tabassum, M. Ahmad, M. Afzal, M. Zaki, P. K. Bharadwaj, *J. Photochem. Photobiol. B* **2014**, *140*, 321.

[53] F. J. Fard, Z. M. Khoshkhoo, H. Mirtabatabaei, M. R. Housaindokht, R. Jalal, H. E. Hosseini, M. R. Bozorgmehr, A. A. Esmaeili, M. J. Khoshkholgh, *Spectochim. Acta A* **2012**, *97*, 74.

[54] J. W. Liang, Y. Wang, K. J. Du, G. Y. Li, R. L. Guan, L. N. Ji, H. Chao, *J. Inorg. Biochem.* **2014**, *141*, 17.

[55] H. L. Wu, H. Wang, X. L. Wang, G. L. Pan, F. R. Shi, Y. H. Zhang, Y. C. Bai, J. Kong, *New J. Chem.* **2014**, *38*, 1052.

[56] L. H. Abdel-Rahman, A. M. Abu-Dief, H. Moustafa, S. K. Hamdan, *Appl. Organometal. Chem.* **2017**, *31*, e3555.

[57] J. Lu, Q. Sun, J. L. Li, L. Jiang, W. Gu, X. Liu, J. L. Tian, S. P. Yan, *J. Inorg. Biochem.* **2014**, *137*, 46.

[58] P. Haris, V. Mary, M. Haridas, C. Sudarsanakumar, *J. Chem. Inf. Model.* **2015**, *55*, 2644.

[59] M. Zaki, M. Afzal, M. Ahmad, S. Tabassum, *J. Photochem. Photobiol. B* **2016**, *161*, 318.

[60] M. A. Rizvi, M. Zaki, M. Afzal, M. Mane, M. Kumar, B. A. Shah, S. Srivastav, S. Srikrishna, G. M. Peerzada, S. Tabassum, *Eur. J. Med. Chem.* **2015**, *90*, 876.

How to cite this article: Qi Y-Y, Liu Y-X, Gan Q, Xiong Y-H, Mao Z-W, Le X-Y. Three new mixed-ligand copper(II) complexes containing glycyl-L-valine and N,N-aromatic heterocyclic compounds: Synthesis, characterization, DNA interaction, cytotoxicity and antimicrobial activity. *Appl Organometal Chem*. 2017;e4126. https://doi.org/10.1002/aoc.4126